water

MDPI

Article

A Comparative Study of GRACE with Continental Evapotranspiration Estimates in Australian Semi-Arid and Arid Basins: Sensitivity to Climate Variability and Extremes

Hong Shen [1,2,*], Marc Leblanc [1,3,4], Frédéric Frappart [5,6], Lucia Seoane [5], Damien O'Grady [1], Albert Olioso [7] and Sarah Tweed [3]

1 Centre for Tropical Water Research & Aquatic Ecosystem Research (TropWATER), James Cook University, 4870 Cairns, Australia; marc.leblanc@univ-avignon.fr (M.L.); damien.ogrady@my.jcu.edu.au (D.O.)
2 State Key Laboratory of Hydro-Science and Engineering, Department of Hydraulic Engineering, Tsinghua University, Beijing 100084, China
3 Research Institute for the Development, UMR G-EAU, 34000 Montpellier, France; sarah.tweed@ird.geau.fr
4 Hydrogeology Laboratory, UMR EMMAH, University of Avignon, 84000 Avignon, France
5 Géosciences Environnement Toulouse (GET)—UMR5563, CNRS, IRD, Université de Toulouse UPS, OMP-GRGS, 14 Avenue E. Belin, 31400 Toulouse, France; frederic.frappart@legos.obs-mip.fr (F.F.); lucia.seoane@get.obs-mip.fr (L.S.)
6 Laboratoire d'Etudes en Géophysique et Océanographie Spatiales (LEGOS)—UMR5566, CNES, CNRS, IRD, Université de Toulouse UPS, OMP-GRGS, 14 Avenue E. Belin, 31400 Toulouse, France
7 UMR EMMAH, INRA—University of Avignon, 84000 Avignon, France; albert.olioso@inra.fr
* Correspondence: hongshen@mail.tsinghua.edu.cn; Tel.: +86-15652623660

Received: 27 January 2017; Accepted: 30 July 2017; Published: 5 September 2017

Abstract: This study examines the dynamics and robustness of large-scale evapotranspiration products in water-limited environments. Four types of ET products are tested against rainfall in two large semi-arid to arid Australian basins from 2003 to 2010: two energy balance ET methods which are forced by optical satellite retrievals from MODIS; a newly developed land surface model (AWRA); and one approach based on observations from the Gravity Recovery and Climate Experiment (GRACE) and rainfall data. The two basins are quasi (Murray-Darling Basin: 1.06 million km^2) and completely (Lake Eyre Basin: 1.14 million km^2) endorheic. During the study period, two extreme climatic events—the Millennium drought and the strongest La Niña event—were recorded in the basins and are used in our assessment. The two remotely-sensed ET products constrained by the energy balance tended to overestimate ET flux over water-stressed regions. They had low sensitivity to climatic extremes and poor capability to close the water balance. However, these two remotely-sensed and energy balance products demonstrated their superiority in capturing spatial features including over small-scale and complicated landscapes. AWRA and GRACE formulated in the water balance framework were more sensitive to rainfall variability and yielded more realistic ET estimates during climate extremes. GRACE demonstrated its ability to account for seasonal and inter-annual change in water storage for ET evaluation.

Keywords: evapotranspiration; GRACE; land surface model; water balance; energy balance; Australia

1. Introduction

Evapotranspiration (ET) governs water and energy exchange between the atmosphere and the Earth's surface [1]. Globally, more than half of the solar energy absorbed by the land surface is used for evaporation and transpiration [2]. Annually, approximately 60% of the water precipitated over

land returns to the atmosphere via the ET process [3]. This percentage could even reach more than 90% in some semi-arid and arid regions such as inland Australia [4,5]. Accurate ET quantification, especially at a catchment or basin scale, is necessary for water resources allocation and irrigation schedule design [6,7]. It is also beneficial for understanding regional climate change and hydrological interactions [8,9].

Numerous continental or global ET datasets (or products) have been produced (e.g., [1,10–17]); they represent the prevailing methods relying on satellite retrievals [18–20], upscaling ground observations [1,9], or simulations from land surface models (LSMs) [16,21], global general circulation models [15,21], and atmospheric reanalysis [1,15]. The mechanisms lying behind these ET estimates/models are usually either based on the energy balance (e.g., Penman–Monteith equation, residual method of surface energy balance, and flux tower measurements) or water budget (e.g., catchment water balance method) [22]. Due to the discrepancy in model structure, forcing datasets, parameterization, upscaling schemes, calibration strategies, as well as validation sources, contemporary ET products/models in and/or between the same categories may have a poor agreement [16,23,24]. Vinukollu et al. [1] reported that the largest uncertainties were found in transition zones between humid and dry regions. Hu et al. [25] also found large spatial inconsistency between two ET remote sensing (RS) datasets (MODIS and LSA-SAFMSG) in some semi-arid regions in Europe. Long et al. [16] showed that two RS ET estimations (from MODIS and AVHRR) behaved abnormally higher than LSM during extremely dry conditions.

In water-limited regions, ET estimates based on the energy balance method could be questionable, as they highlight the energy rather than the water to be the dominant factor in controlling the ET process. Some studies have commented that RS ET products/models may not be sensitive to soil moisture and water deficit [7,26,27]. The use of thermal infrared for forcing surface energy balance models with surface temperature was usually providing coherent estimation of ET and water stress [18,23,28–30]. However, up to now, no dataset of ET derived from thermal infrared data are available at the continental or global scale. In addition, eddy covariance tower observations (constrained by energy balance at field/paddock scales and assuming homogeneous landscapes within an image pixel) are commonly employed as an independent source in large-scale ET validation, which may not be able to fully uncover the deficiency in energy-balance-constrained (RS-based) ET products.

From the points above, semi-arid and arid basins are interesting regions to spot the potential weaknesses of current ET products; the catchment water balance method would be an ideal approach for ET estimation or validation under dry conditions. GRACE satellites make the change in terrestrial water storage (ΔS) detectable at inter- or intra-annual scales [31,32], which further assist the basin-scale ET inter-comparison [33,34]. In this study, we introduced ET estimates derived from regional GRACE solutions (with a higher spatial resolution and less "striping" noises) as an independent source, to compare with three other (two RS-based and one LSM-based) sets of ET products over two large Australian semi-arid and arid basins. Our objective is to assess their overall performance and sensitivity to rainfall variability. To our knowledge, few studies have specifically targeted the water-limited basins to examine the reliability of large-scale ET products.

2. Materials and Methods

2.1. Study Areas

The Murray-Darling Basin (MDB) and Lake Eyre Basin (LEB) were chosen as study areas (Figure 1). Both basins are sufficiently large to meet the minimum spatial resolution of GRACE. The Lake Eyre basin is endorheic, while the Murray-Basin can be considered as sub-closed since there has been no or very limited outflow to the ocean in the past two decades [35,36]. In both basins, ET is the dominating process redistributing the precipitation.

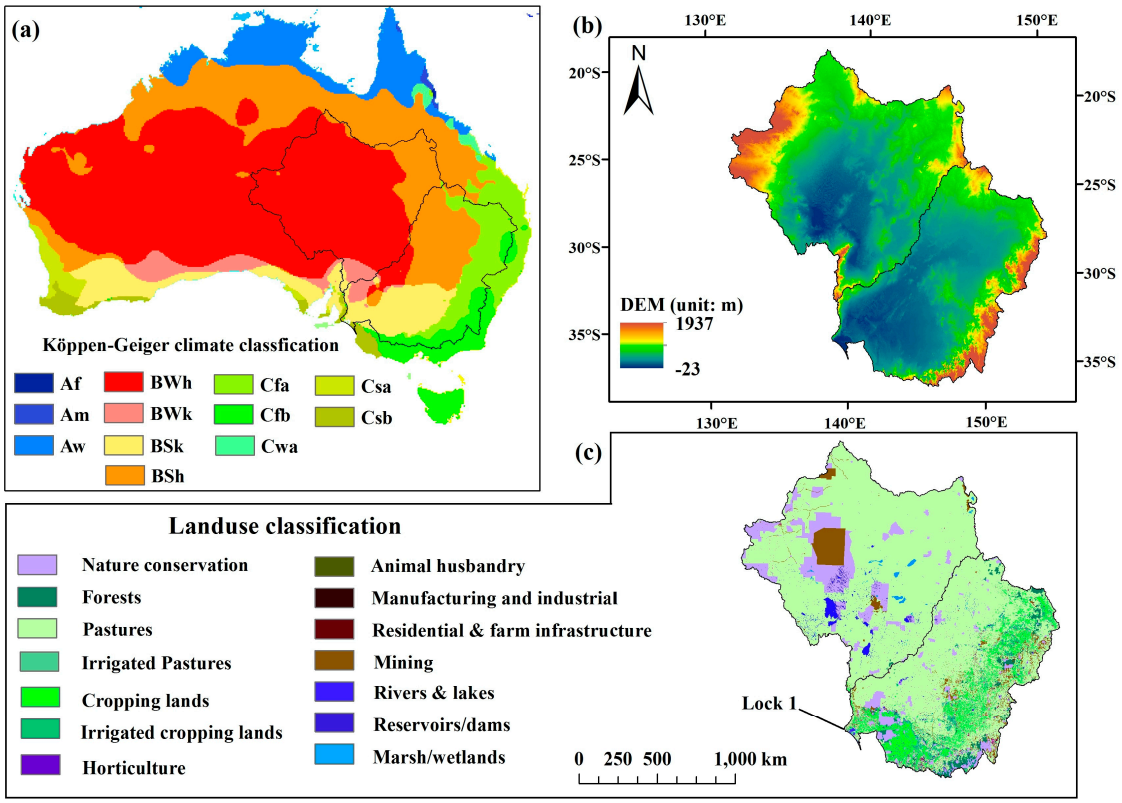

Figure 1. (**a**) Location map of the Murray-Darling and Lake Eyre Basin with climate zone according to the Koppen–Geiger classifications (adapted from [37]): A, equatorial; B, arid; C, warm temperate; W, desert; S, steppe; f, fully humid; s, summer dry; m, monsoonal; w, winter dry; h, hot arid; k, cold arid; a, hot summer; b, warm summer. (**b**,**c**) Digital elevation model (DEM) and land use maps were accessed from [38,39], respectively.

The Lake Eyre Basin (1.14 million km^2) encompasses 81.5% hot dessert (arid climate) and ~15% hot steppe (semi-arid climate). Rainfall within the basin varies widely and is usually unable to meet the atmospheric demand. The annual rainfall over the arid region of the LEB barely reaches 200 mm/year while the north-east edge receives rainfall of up to 700 mm/year under the influence of infrequent tropical storms [40]. The annual potential evaporation (PET) averaged from 1961 to 1990 is of 1453 mm/year (sourced from Australian Bureau of Meteorology data). Floods in the basin are ephemeral and extremely variable [41]. Flows and floodwaters that form during heavy rainfall events carry only 1% of total rainfall; a large fraction (~99%) of rainfall is lost through evaporation and transpiration [35].The Murray-Darling Basin (1.06 million km^2) contains a transition from subtropical to dry arid climate. Rainfall distributions within the basin vary greatly, decreasing from the south-eastern and eastern boundaries (between 600 and 800 mm) towards its western and north-western boundaries (between 100 and 300 mm). The average annual PET was 1236 mm/year (1961–1990). The basin consists of three large river systems and ~30,000 wetlands [42]. As the country's food bowl, ~80% of its area is used for agriculture [43]. Nearly half the surface water is redistributed by irrigation [35]. Many areas in the basin have little or no regular runoff [36,44]; the water levels were reduced to historically low levels during the Millennium Drought from mid-1990s to 2009 [45,46].

2.2. Datasets and Methods

2.2.1. Rainfall, Potential Evaporation, and Discharge Data

Rainfall data, provided by the Australian Bureau of Meteorology (BoM, Melbourne, Australia, data access: [47]), were used for two purposes: (1) to be used with GRACE's measurements to obtain

basin-scale ET estimates through the water balance equation; (2) to evaluate ET datasets and identify their potential deficiencies. The rainfall data is a gridded daily product interpolated from weather station observations [48].

In addition, potential evaporation (hereafter, denoted as E_p) data was obtained from Australian Water Availability Project (AWAP, Canberra, Australia, data access: [49]). Within the Priestley–Taylor framework, E_p was forced by the gridded meteorological data obtained from BoM [50]. A comparison of rainfall with potential evaporation gives a first indication of areas that are mainly controlled by the availability of water versus energy. Both the rainfall and E_p datasets have a spatial resolution of $0.05^\circ \times 0.05^\circ$, and are available from January 2003 to December 2010.

We took the Lock 1 discharge measurements (see the location in Figure 1c) as the river outflow from the MDB. The data was originally archived as daily records (accessed from: [51]), and were further aggregated to monthly equivalent water height (mm/month) divided by total basin area. The LEB is a completely closed basin and no discharge data were required for this basin.

2.2.2. Model-Based ET Estimates

Three continental modelled ET products were used in this study: PT-CMRS, PM-Mu (a.k.a. MOD16), and AWRA-L. They vary in approach, data inputs, and ground calibration (see Table 1). To make these datasets consistent in time and space, ET results sourced from the three models were converted into monthly values from 2003 to 2010 at 0.05° (~5 km) spatial resolution. A brief summary of the forcing datasets, mechanism, and the major features for each ET model is given in Table 1.

- PT-CMRS model

The model. forced by MODIS retrievals and gridded meteorological datasets, was modified based on the Priestley–Taylor (PT) formula ([52]; see Equation (1)) to dynamically represent the actual ET variations over the Australian continent (hereafter, denoted as "PT-CMRS").

$$\mathrm{ET}_{\text{PT-CMRS}} = \alpha \frac{\Delta}{\Delta + \gamma}(R_n - G), \tag{1}$$

where R_n is the surface net radiation(MJ m^{-2} d^{-1}); G is the soil heat flux (MJ m^{-2} d^{-1}); Δ is the slope of the curve relating saturation water vapor pressure to temperature (kPa K^{-1}); γ is the psychometric constant (kPa K^{-1}). The prominent advantage associated with the PT method is that it does have limited input data requirement; wind speed is not compulsory in the model.

The developers replaced the original empirical constant α = 1.26 with a flexible scaling factor formulated by the Enhanced Vegetation Index (EVI) and the Global Vegetation Moisture Index (GVMI) [53]. This scheme allows GVMI to separate surface water bodies against bare soil when EVI is low and to detect vegetation water content when EVI is high. Also, the PT-CMRS model accounts for precipitation interception. This model was calibrated at seven flux sites in Australia and validated in 227 catchments. Readers can refer the details about the PT-CMRS ET model from [45]. Data can be downloaded from: [54].

Table 1. Summary of the ET datasets used in this study except for GRACE.

Name	Algorithm	Resolution		Forcing Data		Calibration in Australia
		Temporal	Spatial (°)	Ground Meteorological Inputs	Remote Sensing Inputs	
PT-CMRS	MODIS [1]-based retrievals to scale the PT method	8-day	0.002	SILO [2] (temperature + radiation) datasets	MOD13Q1 + MOD09A1	7 flux sites (two forests, two savannah, a grassland, a floodplain, and a lake)
PM-Mu	MODIS-based retrievals to force the PM method	monthly	0.05	GMAO [3] datasets	MOD12Q1 + MOD13A2 + MOD15A2 + MOD43C1	None
AWRA	Water and energy constrained model	daily	0.05	SILO and BAWAP [4] datasets	AVHRR [5] NDVI [6]	4 flux sites and up to 326 catchments

Notes: [1] Moderate Resolution Imaging Spectroradiometer; [2] SILO datasets were produced by the Department of Environment and Resource Management, Australia; [3] GMAO dataset produced by the NASA Global Modeling and Assimilation Office; [4] BAWAP datasets were produced by the Bureau of Meteorology, Australia; [5] Advanced Very High Resolution Radiometer; [6] Normalized Difference Vegetation Index.

- PM-Mu model ([10,13])

Based on Cleugh's method [10], the MOD 16 ET data set developed by Mu ([13]; denoted here as 'PM-Mu') -integrated MODIS-retrieved leaf area index (LAI) into the Penman-Monteith (PM) equation ([55]; see Equation (2)), and improved the estimation of surface resistance and soil evaporation [13].

$$\mathrm{ET}_{\mathrm{PM}-Mu} = \frac{(R_n - G)\Delta + \rho_a c_p (e_s - e_a)/r_a}{\lambda[\Delta + \gamma(1 + r_s/r_a)]}, \quad (2)$$

where ρ_a is the mean air density at constant pressure (kg m^{-3}); c_p is the specific heat of air at constant pressure (MJ kg^{-1} K^{-1}); $(e_s - e_a)$ is the water vapor pressure deficit between the saturated air pressure and the actual air pressure (kPa); r_s and r_a represent the surface/aerodynamic resistance (m s^{-1}); λ is latent heat of evaporation (MJ m^{-2} d^{-1}).

Further modifications were described in [19]. The dataset is available at global scale. Results have been tested at global and flux-site scales. Data can be downloaded from: [56]. The PM model is process-based and constrained by energy balance. It requires considerably more input data than the PT model; some of this data (especially the wind speed) are barely available over large basins or regions. However, meteorological data have been obtained from atmospheric model reanalysis or gridded meteorological datasets.

- ET estimates from AWRA-L land surface model

The AWRA (Australian Water Resources Assessment) ET output (denoted as "AWRA") was produced by a multi-model system simulating hydrological processes and dynamics in landscape, river and groundwater systems, and water use all over Australia [57]. This system is jointly developed by the BoM and the Commonwealth Scientific and Industrial Research Organization (CSIRO). Either the PM or the PT functions were used, depending on the availability of wind speed data [58]. Within each cell, ET is summarized as:

$$E = E_i + E_t + E_g + E_s + E_r, \quad (3)$$

where E_t is vegetation transpiration; E_i, E_r, E_g, and E_s are evaporation from rainfall interception, open water bodies, groundwater, and soil profiles, respectively. AWRA ET estimates balance the requirement between water/energy conservation and data unavailability. However, the model neglects lateral water flows, which leads to an underestimation of ET over areas receiving inflows, such as wetlands, floodplains, and irrigated farmland. Gauged runoff and eddy covariance flux tower observations were used to visually fit some components and parameters of the model.

2.2.3. ET Estimates from GRACE Rainfall and Discharge Observations

A number of studies have derived ET estimates from GRACE observations in large basins, e.g., [11,33,34].

Here we computed ET estimates using regional GRACE solutions which are characterized by reduced north-to-south striping (using constrained regularization) and no contamination from other parts of the world [59,60]. Several studies over different continents—South America [61], Australia [62], and Africa [63]—demonstrated that this regional approach offers a reduction of both north-south striping due to the distribution of GRACE satellite tracks and temporal aliasing of correcting models that are present in the global GRACE solutions. GRACE regional solutions were available at a spatial resolution of $2^\circ \times 2^\circ$ from 4 July 2003 to 3 December 2010 at intervals of 10 days [62]. Change in the basin water storage (ΔS) is calculated as the difference between two successive GRACE terrestrial water storage anomalies (TWSA) against the average (ΔTWS):

$$\Delta TWS = \Delta S = TWS_{t2} - TWS_{t1}. \quad (4)$$

Using the water balance equation at basin-scale, ET was obtained as the difference between the total amount of rainfall over the basin (P), the river discharge at the outlet (Q) and the change in ΔS over a specific time period Δt:

$$\mathrm{ET} = P - Q - \Delta S, \tag{5}$$

To be consistent with the above modelled ET datasets, calculations were performed over 30-day time period. Missing data from 20 January 2004 to 29 January 2004 were linearly interpolated. Combining GRACE ΔTWS observations and BoM rainfall datasets, monthly basin-average ET estimates over the MDB were computed using Equation (5) with all variables set. However, due to the fact that Q is unavailable at gridded-cell scale, GRACE ET maps were approximated as ($P - \Delta S$) with Q assumed to be negligible. This operation was also applied to the LEB.

2.2.4. Evaluation of ET Estimates Using the Budyko Diagram Scheme

Water balance at basin-scale is governed by Equation (5). In the Budyko framework, the nature of the annual water balance is determined by the ratio E/P (evaporation efficiency) as a function of E_p/P (drought index or climatic aridity) accounting for the partition of rainfall between evaporation and runoff [64]:

$$\frac{E}{P} = \left\{ \left[1 - \exp\left(-\frac{E_p}{P}\right) \right] \frac{E_p}{P} \tanh\left(\frac{P}{E_p}\right) \right\}^{0.5} \tag{6}$$

In extremely dry cases, if a basin is provided with sufficient evaporative energy but limited precipitation, then E will approximate to P; conversely, E will be mainly determined by E_p in a wet basin. These form two asymptotes to constrain the Budyko curve in a boundary. A Budyko diagram is usually used at long-term average scale. Since GRACE could provide the annual basin water storage change information, we assumed that the Budyko diagram could be valid at inter-annual time step. Annual E and P were presented as Ea and Pa, respectively.

Noticing that the indices of Ea/Pa and E_p/Pa could be sensitive to the different sources of Pa and E_p, we assumed that E_p/Pa would not vary widely as E_p in MDB and LEB is much larger than Pa; Pa is based on measurements from rainfall stations.

3. Results

3.1. Spatial Evaluation

Figure 2 shows the spatial distribution across the two basins of average annual ET for each dataset and average annual rainfall over the 2003–2010 period. The estimated annual ET maps are spatially consistent with corresponding rainfall maps. The highest ET rates were found in south-eastern MDB (>800 mm/year) where the climate is more humid and intense canopy transpiration occurs. The northern parts of MDB and LEB also present a high ET rate of 400–600 mm/year, which is attributed to the strong ET fluxes caused by tropical rainstorms during the summer. Controlled by an arid climate, 100–200 mm/year of rainfall, the central part of the LEB and the western MDB show the lowest ET rates of all four datasets.

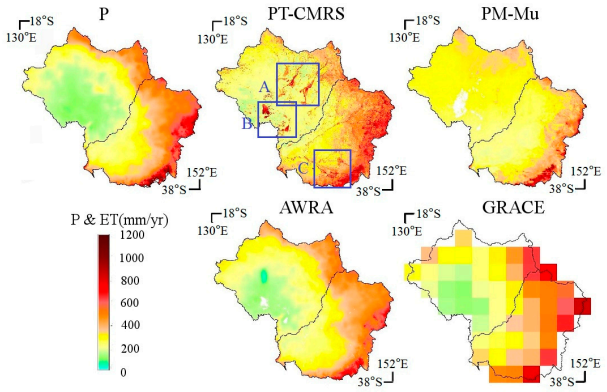

Figure 2. Spatial distribution of mean annual rainfall (P) and mean annual ET derived from PT-CMRS, PM-Mu, AWRA, and GRACE across the Murray-Darling and the Lake Eyre Basins. Boxes A, B, and C show areas that are zoomed in Figure 3.

However, we identified some differences between ET estimates. Over the extremely dry regions of the central LEB (rainfall: 100–200 mm/year), ET estimates from AWRA and GRACE were more reasonable than the values provided by two energy balance constrained methods (PM-Mu and PT-CMRS) which predicted 200–300 mm/year of water lost via ET processes over the central LEB. Over humid regions, PM-Mu estimated an annual ET flux lower than the other three methods.

Figure 3 zooms in three smaller regions (boxes A, B, and C shown in Figure 2) that are prone to inundation (A and B) or irrigation (C). The red patches in contrast to the dry background in PT-CMRS represent the high-ET patterns over irrigated areas as well as flood plains composed of open water bodies and dense forests, demonstrating the dataset's ability to capture relatively small ET features and heterogeneities over those landscapes. This ability is mostly attributed to the integration of MODIS-based EVI and GVMI indices in PT-CMRS [53]. Although it was also driven by MODIS optical products, PM-Mu did not clearly present those small-scale ET features in space. AWRA also considered ET flux from canopy cover and open waters as well as saturated soil. Nevertheless, its coarse gridding system and fractional index parameterization for different land covers make the model homogenize those landscape features.

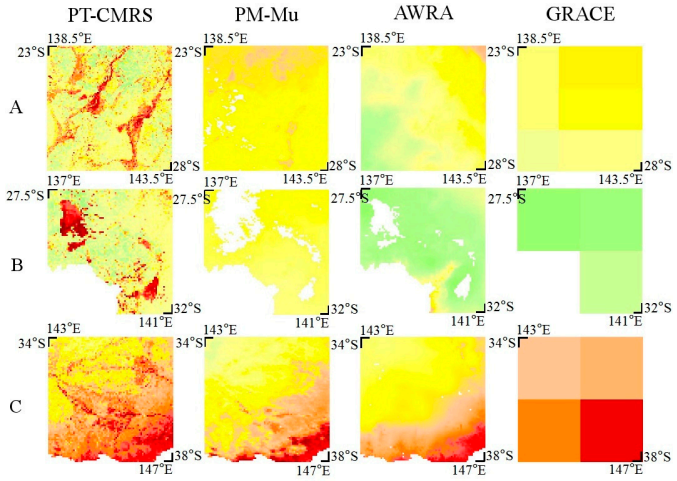

Figure 3. Zoom in mean annual ET values from the four models over three smaller regions (boxes A, B, and C shown in Figure 2) that are prone to inundation or irrigation.

3.2. Temporal Evaluation

3.2.1. Seasonal Variations

Table 2 shows the mean seasonal ET estimates and corresponding rainfall averaged over the period 2003–2010 and the fractions of ET to rainfall. The four methods used to estimate ET in this study were able to capture the seasonal ET patterns in each basin. LEB is much drier (has little rainfall against high potential evaporation requirement) than the MDB. Therefore, it is likely that the ET fluxes in the LEB is lower than in the MDB through the four seasons. However, in a comparison of the magnitude of seasonal ET to rainfall, the four methods behaved inconsistently. Again, seasonal PM-Mu estimates were constantly lower than other ET datasets in MDB, with the lowest ratio of 0.4 found in winter. The ratios of ET/P are frequently above 1.0 in PT-CMRS and PM-Mu during the dry seasons in LEB; the largest ratios (1.5 for PT-CMRS and 1.6 for PM-Mu) are observed in autumn, indicating that estimated ET is greater than the rainfall by 20–30 mm on average. This is also clearly shown by the large gap in Figure 4b. Both methods PM-Mu and PT-CMRS actually did not use the input data directly related to water balance (as rainfall or groundwater storage variations) or to water stress (as thermal infrared data) but mainly relied on the evolution of vegetation as monitor from remote sensing data. Inclusion of thermal data could have picked some low and high moisture conditions. LAI alone may not capture the variation on soil moisture, typically when the bare soil evaporation becomes significant after rainfall or under extreme dry conditions. By comparison, constrained by rainfall in its algorithm, mean seasonal ETs estimated by AWRA and GRACE were closer to the rainfall levels, with their ratios falling into a range of 0.7–1.2.

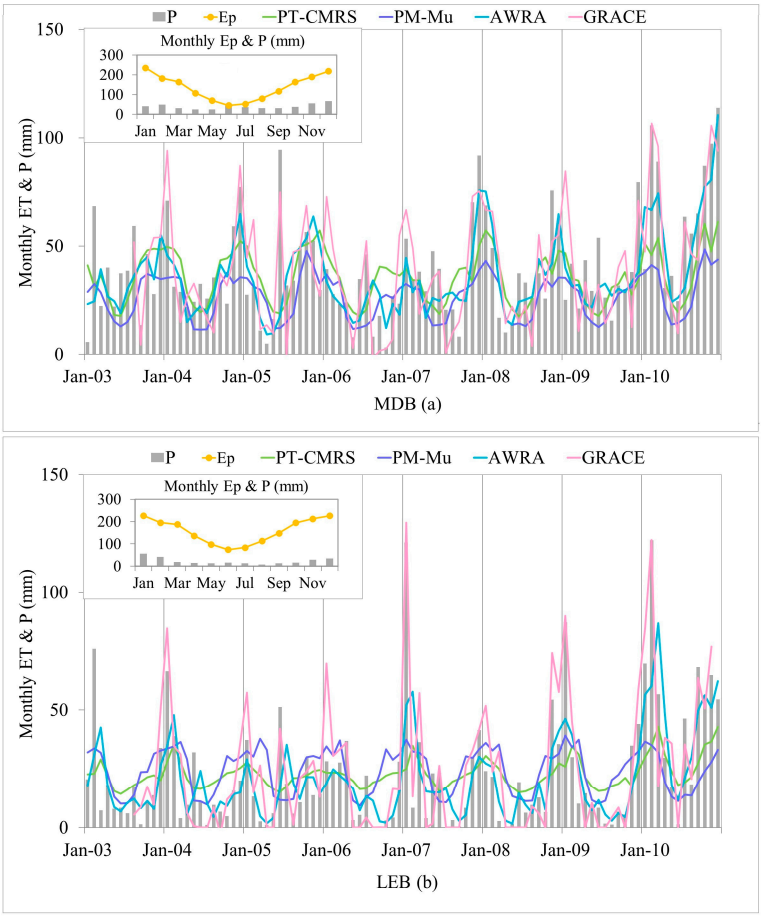

Figure 4. Monthly ET time series derived from the four ET datasets with rainfall and potential evaporation (E_p) over the MDB (**a**) and LEB (**b**) from 2003 to 2010.

Table 2. Mean seasonal ET from the four ET models and their ratio to rainfall (denoted as P) for the period 2003–2010.

Basin	ET Model	Spring (September–November)			Summer (December–February)			Autumn (March–May)			Winter (June–August)		
		ET (mm)	P (mm)	Ratio	ET (mm)	P (mm)	Ratio	ET (mm)	P (mm)	Ratio	ET (mm)	P (mm)	Ratio
LEB	PT-CMRS	68.7	57.9	1.2	83.1	132.4	0.6	68.9	45.2	1.5	51.4	36.9	1.4
	PM-Mu	80.1		1.4	99.9		0.8	72.5		1.6	36.3		1.0
	AWRA	50.1		0.9	102.5		0.8	55.5		1.2	40.3		1.1
	GRACE	63.5		1.1	165.0		1.2	49.9		1.1	24.2		0.7
MDB	PT-CMRS	129.6	125.6	1.0	137.4	156.3	0.9	87.3	81.7	1.1	72.7	112.0	0.7
	PM-Mu	102.2		0.8	105.8		0.7	65.9		0.8	47.2		0.4
	AWRA	126.5		1.0	145.5		0.9	77.3		1.0	85.4		0.8
	GRACE	120.1		1.0	192.8		1.2	77.1		0.9	79.8		0.7

In Figure 5, ET estimates during the peak Millennium Drought and the La Niña spell are compared with mean monthly values averaged over August 2003 to July 2010. The peak of the Millennium Drought occurred in August to December 2006 for the MDB and January to May 2008 for the LEB; monthly rainfall reduced by 20–40 mm on average. The La Niña caused abnormally high rainfall over the MDB (December 2009–May 2010) and the LEB (November 2009–April 2010). Four ET methods responded to the climate extremes dynamically. The smaller the anomalies were, the more similar the modelled ET estimates were to their multi-year average, and vice versa. Small anomalies were found in PT-CMRS and PM-Mu, which implies that ET estimates reproduced by these two energy balance constrained models do not apparently vary during the extremely wet or dry spells. AWRA and GRACE performed sensitively to climatic extremes. In spite of some spikes, the GRACE-based ET product tended to provide a relatively high/low ET with a magnitude consistent with rainfall.

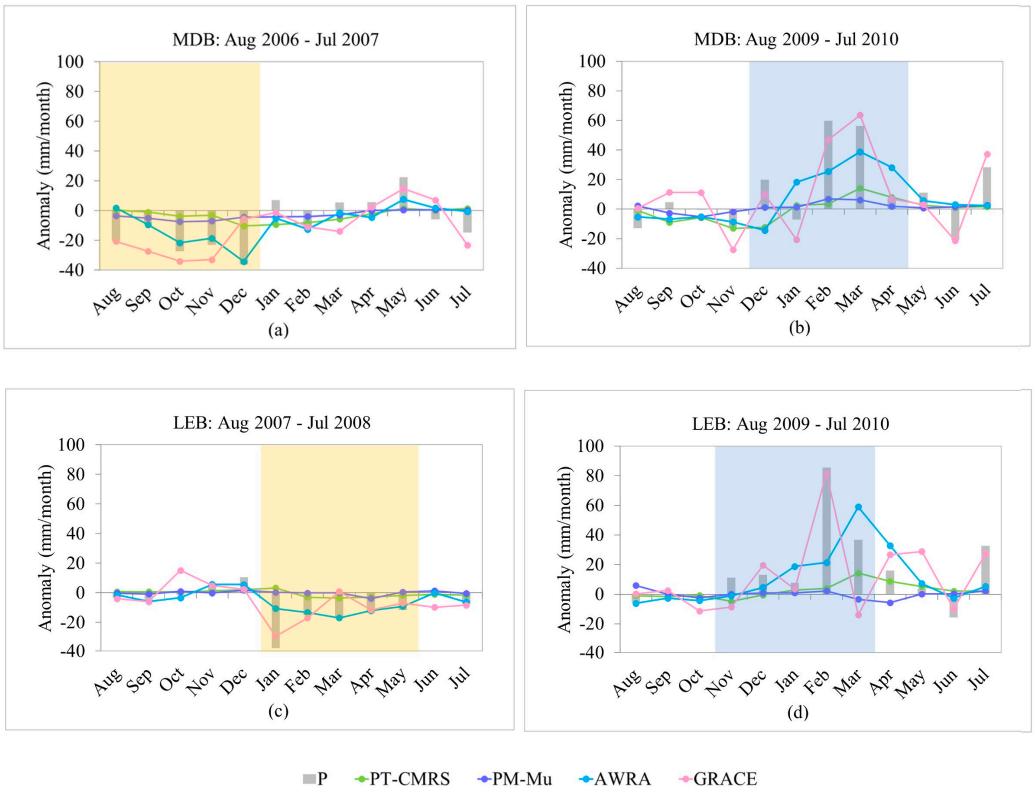

Figure 5. Monthly ET anomalies during extreme climatic events: peak of Millennium drought and La Niña computed as deviation to monthly averages for the whole study period (August 2003 to July 2010). MDB (**a**) and LEB (**c**) during the peak of the Millennium drought; MDB (**b**) and LEB (**d**) during the La Niña period.

3.2.2. Inter-Annual Variations

Inter-annual comparisons were performed at basin-scale to test the response of the four ET datasets. Figure 4 shows monthly ET estimated by the four ET methods over the MDB and LEB from 2003 to 2010 (GRACE ET starts from August 2003), against the rainfall and potential evapotranspiration (E_p) for the same period. At monthly time steps, the correlation coefficients (R) were computed to measure the agreement between each ET pair as well as their sensitivity to rainfall.

Monthly E_p rates (ranging from 50 to 250 mm/month in MDB and from 80 to 250 mm/month in LEB) were always higher than the rainfall levels throughout the study period, indicating water-limited conditions. In that case, ET fluxes in our study areas is predominantly controlled by water availability rather than by energy. Two energy-based models show a quite low linear correlation with rainfall; $R_{PT\text{-}CMRS}$ = 0.35 and $R_{PM\text{-}Mu}$ = 0.41 for the MDB, and $R_{PT\text{-}CMRS}$ = 0.51 and $R_{PM\text{-}Mu}$ = 0.37 for the LEB.

Remarkable differences can be found during wet ($ET_{PT\text{-}CMRS}$ and $ET_{PM\text{-}Mu} < P$) or dry spells ($ET_{PT\text{-}CMRS}$ and $ET_{PM\text{-}Mu} > P$; particularly in LEB). By comparison, AWRA has high correlation with rainfall in both basins, $0.7 < R < 0.8$. AWRA and GRACE ET estimates were closer to rainfall levels (especially GRACE) due to the fact that they were forced by rainfall data. They also had a good consistency with each other: $R_{MDB} = 0.67$ and $R_{LEB} = 0.69$. Although PT-CMRS had a higher linear relationship with AWRA ($0.77 \leq R_{MDB/LEB} \leq 0.79$), the amplitude of the PT-CMRS was significantly lower than AWRA during the extreme seasons. In general, the two energy-balanced products exhibited similar patterns at monthly time steps, and displayed large differences with AWRA and GRACE-based ET in dry and wet periods. PM-Mu was systematically lower than other ET sources in MDB.

Figure 6 presents the capability of each ET dataset in capturing ET variations in different hydrological years. PM-Mu constantly provided the lowest ET estimates over the MDB; a common short of ~100 mm/year was found when compared to PT-CMRS. Compared to AWRA and GRACE estimates, PT-CMRS provided larger values over the MDB in dry hydrological years but lowest values during wet years (e.g., August 2009–July 2010; impacted by La Niña event). ET overestimation by the two energy balance constrained models was commonly observed in the LEB, with annual ET flux twice or larger than the rainfall during the extremely dry hydrological year of August 2004–July 2005 and August 2007–July 2008. Moreover, these two estimates did not exhibit any response to rain variations from year to year and provided almost constant annual values. Constrained by the water balance equation, AWRA and GRACE showed a good sensitivity to annual rainfall variations both in timing and magnitude. GRACE-derived ET estimates at annual scales showed larger inter-annual variations than AWRA over the MDB (with ET larger than rain for some years), while very similar results were obtained over the LEB.

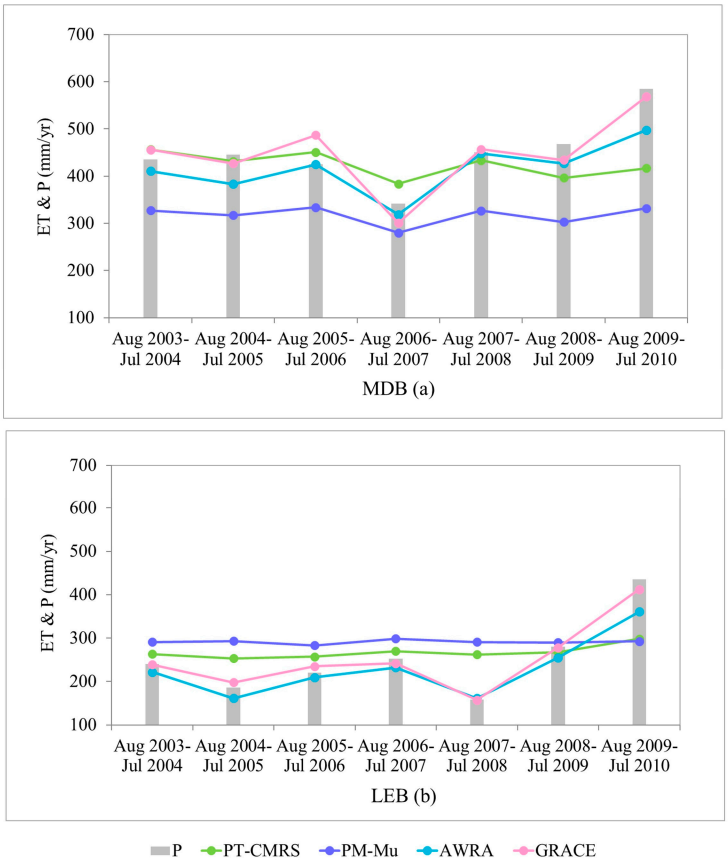

Figure 6. Annual rainfall and ET computed in each hydrological year from August 2003 to July 2010 for the MDB (**a**) and the LEB (**b**).

A Budyko diagram was used to confirm that ET fluxes in our two basins were determined by water availability rather than the energy factor. Estimates were plotted in the Budyko diagrams to examine the variation of the water closure property across hydrological years (Section 2.2.4).

The aridity indices in the Budyko diagrams (Figure 7) confirm that LEB is more arid than MDB (LEB: 4.0 < E_p/Pa < 11.5; MDB: 2.7 < E_p/Pa < 5.0). In MDB, Ea/Pa ratios estimated by PM-Mu were sitting in a range 0.5–0.8, demonstrating a systematically low percentage of rainfall transforming into ET. For the same basin, PT-CMRS had some Ea/Pa values lying beyond y = 1 in some dry years (larger E_p/Pa), manifesting a slight outperformance of PT-CMRS ET during drought conditions. Such a phenomenon was more apparent in the LEB. The dryer the year in the LEB (E_p/Pa > 10), the more unrealistically the PM-Mu and PT-CMRS estimates; Ea/Pa ratios reached 1.8 (PM-Mu) and 1.7 (PT-CMRS) when LEB received the lowest annual rainfall (158.6 mm/year) from August 2007 to July 2008. By comparison, Ea/Pa predicted by the two water-balance-constrained methods (GRACE and AWRA) were much closer to the asymptotic curve. AWRA and GRACE predicted 85.1% and 97.5% of rainfall lost via evaporation in both basins during the wettest year August 2009–July 2010, respectively; that is to say, 15% (from AWRA) and 2.5% (from GRACE) of rainfall would be converted into runoff and exit the basin or be stored in the aquifer.

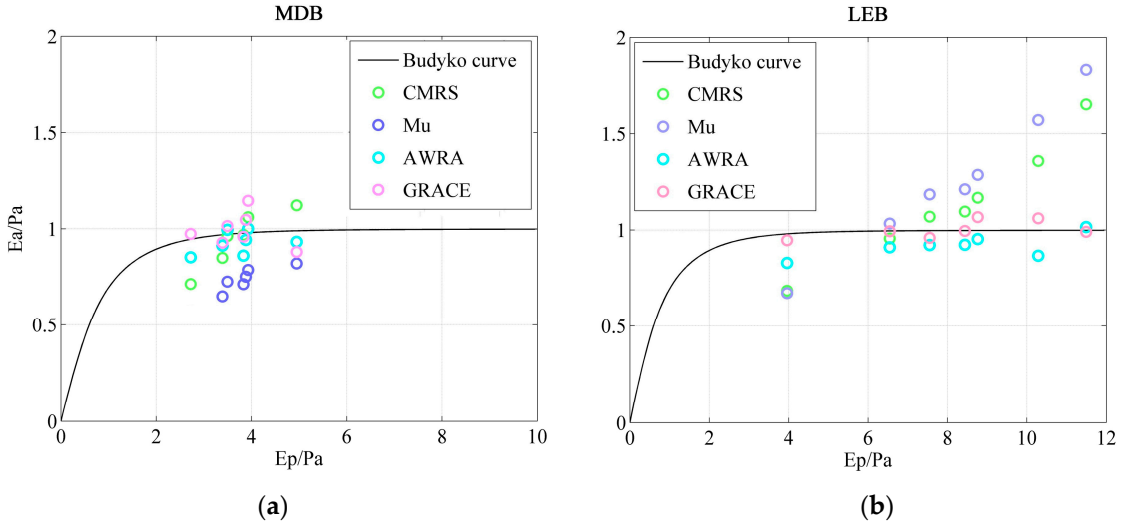

Figure 7. Budyko diagrams for the MDB (**a**) and the LEB (**b**). Ea represents the annual ET estimated by PT-CMRS, PM-MU, AWRA and GRACE. Pa is annual rainfall. E_p is potential evapotranspiration based on the Priestley–Taylor method. All the terms were computed for each hydrological annual year from 2003 to 2010.

4. Discussion

Catchment/basin water balance method provides the simplest way to solve ET estimation by meeting only three water budget components as its input variables. However, the component of ΔS is usually the hardest part to access or measure. In most cases, the common way to address the absence of ΔS is to regard it as negligible over a long-term period [31,32,65]. But when it comes to the annual or inter-annual scales, neglecting of ΔS would lead to an imbalance of water budget equation [66–68]. In fact, short-term ΔS can be a crucial component in water budget, particularly when a basin meets climate extremes. Time series of ΔS anomaly over the MDB and the LEB exhibits large annual (several tenths of mm of equivalent water height) and inter-annual variations (with a decrease from 2003 to 2009 and an increase since) between 2003 and 2010 (Figure 8). Table 3 presents GRACE-derived annual ΔS in different water years over the MDB and LEB: remarkable changes in water storage occurred during August 2005–July 2006 (a water deficit of −20.3 and −70.4 mm/year occurred in LEB and MDB, respectively) and August 2009–July 2010 for LEB only (a water gain by 31.8 mm/year). Such a

water loss or gain in ΔS would take up 10–20% of total annual rainfall for both basins. By including GRACE-estimated ΔS, the closure of the basin water balance equation is improved; what's more, the phase and amplitude of the annual and seasonal cycle of ET can be ascertained [69].

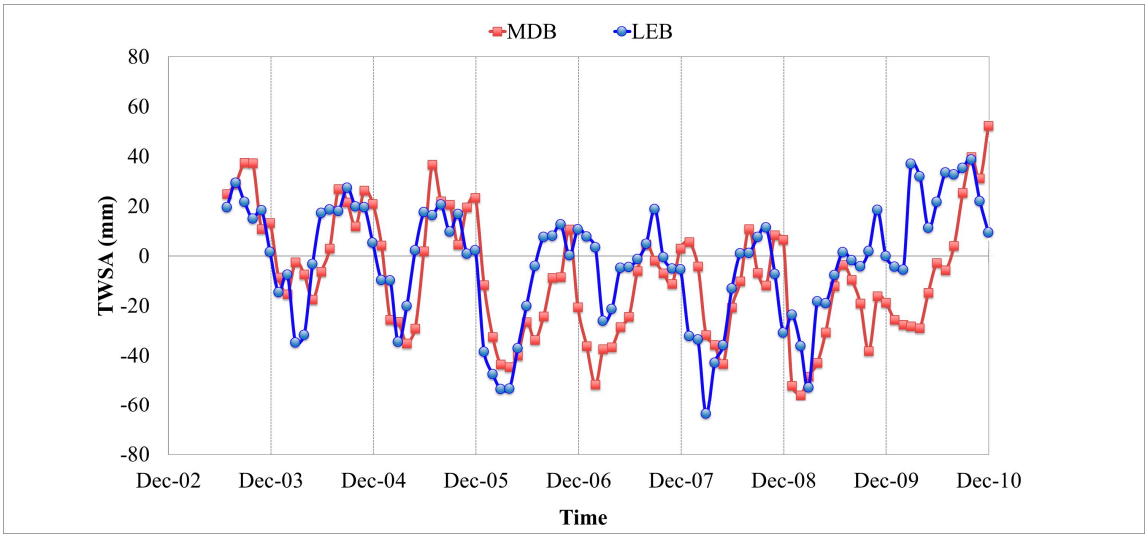

Figure 8. Time series of terrestrial water storage anomaly (TWSA) between 2003 and 2010 from GRACE regional solutions over the MDB (red) and the LEB (blue).

Table 3. Annual changes in terrestrial water storage (ΔS) over the MDB and the LEB between 2003 and 2010. Annual ΔS was computed as the TWS difference between the end month (August) and the start month (July) within a hydrological year (unit: mm/year).

Basin	August 2003 –July 2004	August 2004 –July 2005	August 2005 –July 2006	August 2006 –July 2007	August 2007 –July 2008	August 2008 –July 2009	August 2009 –July 2010	Average
LEB	−0.9	−2.3	−20.3	2.7	2.2	0.6	31.8	2.0
MDB	−21.9	33.6	−70.4	27.7	−4.2	−6.7	−2.2	−4.4

In terms of the uncertainty of GRACE-based ET estimates, they are largely dependent on the quality of GRACE TWSA and thus computed ΔS. A previous study using regional GRACE solutions over Australia found an uncertainty of 19.1 mm when computing the standard deviation of the TWSA over a xeric region [52]. Another major source of uncertainty associated with GRACE ET estimates is attributed to the quality of rainfall data. Usually, arid and semi-arid basins have poor rainfall monitoring networks. In our case, MDB has much denser monitoring networks than LEB does; the latter has a large unpopulated region without rainfall stations [63]. At basin scales, the RMSE calculated between BoM and TRMM 3B43 rainfall datasets are 3.0 and 27.4 mm/month for MDB and LEB, respectively. By blending gauge records with ancillary rainfall data, such as radar and satellite measurements or an ensemble method, may improve the accuracy of rainfall input data [63,64].

Optical satellite imagery allows landscape conditions such as vegetated surface, biome types, and surface standing waters to be distinguishable at unprecedentedly high spatiotemporal resolution (e.g., 0.05° and 8/16 days for MODIS), which facilitates an enhancement in simulating large-scale ET processes. For example, an integration of RS vegetation index (VIs, including LAI, NDVI, and EVI) allows for a separation between plant transpiration and soil evaporation, as well as for adding the canopy rainfall interception component into ET modelling. In our study, PM-Mu employs a complex and process-based scheme to address vegetation transpiration and soil evaporation separately; the new version sets up numerous thresholds to define canopy stomatal conditions over biomes and wet canopy [19]. PT-CMRS combines the EVI and GVMI indexes into a simple and dynamic scaling strategy of the Priestley–Taylor framework to deal with transpiration or evaporation from vegetation,

open water bodies, and bare soil; it does consider canopy rainfall interception but merely as a scaled precipitation component. In addition, PT-CMRS ET estimates heavily rely on ground calibration (none of the flux tower sites are distributed in inland dry areas) [53]. Obviously, there is a tradeoff between accuracy and parsimoniousness in ET modelling, as well as a consideration of data availability from ground observations.

In arid and semiarid environments, soil evaporation often makes up the majority of the total ET due to low vegetation coverage. This means that ET models should be able to reflect the relation with soil moisture conditions. Land surface models like AWRA partition precipitation to soil moisture and groundwater systems (other LSMs may not), and thus put a soil moisture constraint onto ET. However, the soil water constraint of energy-based ET products, such as PM-Mu and PT-CMRS, tends to be weak; most models tend to determine ET fluxes by energy factor, in particular based on net radiation estimation rather than by water constraint. Long et al. [16] mentioned that such RS-based ET models only make soil moisture implicitly linked to VIs and atmospheric variables. PM-Mu has soil moisture information indirectly linked to the LAI/NDVI and vapor pressure deficit (VDP); so does PT-CMRS, replaced by EVI and GVMI. These models implicitly assume that vegetation develops in agreement with water availability, which may be true over a long term or "standard" climatic period, but can fail in conditions when drought or rainfall present situations far from average. These models also rely on parameters (e.g., describing stomatal response) that are difficult to assess at large scale, as well as on the accuracy of land use maps. In semi-arid and arid regions, such as MDB and LEB, rain may fall and evaporate directly from bare soil, hence without major influence on vegetation indices and derived ET estimates. That is a potential explanation as to why satellite ET datasets like PT-CMRS and PM-Mu are less sensitive to rainfall/soil moisture and cannot balance well the water budget in these arid and semi-arid environments. Other RS-based ET models rely on the use of thermal infrared data that provide a strong link to water stress and moisture availability and which may improve significantly energy balance estimates. However, today there are no available operational ET products based on thermal infrared, in particular because such models are difficult to implement over large areas such as a continent or even a country. They either rely on a highly accurate characterization of spatial variation of climatic variables (in particular air temperature) or require a very homogeneous climatic zone for implementation.

5. Conclusions

This study, examines the dynamics of continental ET products in water-limited environments. Four ET datasets derived from PT-CMRS, PM-Mu, AWRA, and GRACE were compared in the Murray-Daring and Lake Eyre Basins, against rainfall variations and during climate extremes. Two energy balance constrained ET methods, PT-CMRS and PM-Mu, which are forced by optical satellite retrievals, have poor response to high water variability; they provided unrealistically high ET values (beyond the rainfall) during the drought and low values when rainfall became exceptionally high. This problem can be attributed to the lack of water constraint following water balance. In contrast, AWRA and GRACE are forced by rainfall data, demonstrating their dynamics in addressing the spatial/temporal rainfall variability over water-limited environments. Absolute error associated with each ET product is not directly measurable but a measure of error may be established via a basin-scale comparison with the ensemble mean.

Our results imply that: (1) current ET models based on the energy balance and derived using optical data are not accurate over water-limited areas and that they may need to include further water constraint(s) for ET estimation over arid and semi-arid regions; (2) GRACE observations provide a valuable tool for quantifying basin-scale water storage change at annual or sub-annual scales, as well as an independent source for large-scale ET mapping and validation; (3) a promising way to enhance ET estimation over large water-limited basins/regions may rely on merging high-resolution (but poor in basin-water-balance-constrained) optical RS-based ET products with well water-balance-constrained (but coarse in spatial resolution) GRACE ET estimates [20,70].

Acknowledgments: The authors would like to thank the Murray-Darling Basin Authority and the BoM for providing some of the datasets used in this study. We also thank four anonymous reviewers and the journal's academic editor for their valuable comments that helped us in improving the quality of our manuscript.

Author Contributions: Each co-author contributed to the research published in this paper.

Conflicts of Interest: The authors declare no conflict of interest. The funding agencies had no role in the design of the study, and in the decision to publish.

References

1. Vinukollu, R.K.; Meynadier, R.; Sheffield, J.; Wood, E.F. Multi-model, multi-sensor estimates of global evapotranspiration: Climatology, uncertainties and trends. *Hydrol. Process.* **2011**, *25*, 3993–4010. [CrossRef]
2. Trenberth, K.E.; Smith, L.; Qian, T.; Dai, A.; Fasullo, J. Estimates of the Global Water Budget and Its Annual Cycle Using Observational and Model Data. *J. Hydrometeorol.* **2007**, *8*, 758–769. [CrossRef]
3. L'vovich, M.I.; White, G.F. Use and transformation of terrestrial water systems. In *The Earth as Transformed by Human Action*; Turner, B.L., Ed.; Cambridge University Press: New York, NY, USA, 1990; pp. 235–252.
4. Chirouze, J.; Boulet, G.; Jarlan, L.; Fieuzal, R.; Rodriguez, J.C.; Ezzahar, J.; Er-Raki, S.; Bigeard, G.; Merlin, O.; Garatuza-Payan, J.; et al. Inter-comparison of four remote sensing based surface energy balance methods to retrieve surface evapotranspiration and water stress of irrigated fields in semi-arid climate. *Hydrol. Earth Syst. Sci. Discuss.* **2013**, *10*, 895–963. [CrossRef]
5. Australia. National Water Commission. *Australian Water Resources 2005: A Baseline Assessment of Water Resources for the National Water Initiative*; National Water Commision: Canberra, Australia, 2006.
6. Gowda, P.H.; Senay, G.B.; Howell, T.A.; Marek, T.H. Lysimetric Evaluation of Simplified Surface Energy Balance Approach in the Texas High Plains. *Appl. Eng. Agric.* **2009**, *25*, 665–669. [CrossRef]
7. Senay, G.B.; Leake, S.; Nagler, P.L.; Artan, G.; Dickinson, J.; Cordova, J.T.; Glenn, E.P. Estimating basin scale evapotranspiration (ET) by water balance and remote sensing methods. *Hydrol. Process.* **2011**, *25*, 4037–4049. [CrossRef]
8. Huntington, T.G. Evidence for intensification of the global water cycle: Review and synthesis. *J. Hydrol.* **2006**, *319*, 83–95. [CrossRef]
9. Jung, M.; Reichstein, M.; Ciais, P.; Seneviratne, S.I.; Sheffield, J.; Goulden, M.L.; Bonan, G.; Cescatti, A.; Chen, J.; de Jeu, R.; et al. Recent decline in the global land evapotranspiration trend due to limited moisture supply. *Nature* **2010**, *467*, 951–954. [CrossRef] [PubMed]
10. Cleugh, H.A.; Leuning, R.; Mu, Q.; Running, S.W. Regional evaporation estimates from flux tower and MODIS satellite data. *Remote Sens. Environ.* **2007**, *106*, 285–304. [CrossRef]
11. Ferguson, C.R.; Sheffield, J.; Wood, E.F.; Gao, H. Quantifying uncertainty in a remote sensing-based estimate of evapotranspiration over continental USA. *Int. J. Remote Sens.* **2010**, *31*, 3821–3865. [CrossRef]
12. Leuning, R.; Zhang, Y.Q.; Rajaud, A.; Cleugh, H.; Tu, K. A simple surface conductance model to estimate regional evaporation using MODIS leaf area index and the Penman-Monteith equation. *Water Resour. Res.* **2008**, *44*, W10419. [CrossRef]
13. Mu, Q.; Zhao, M.; Heinsch, F.A.; Liu, M.; Tian, H.; Running, S.W. Evaluating water stress controls on primary production in biogeochemical and remote sensing based models. *J. Geophys. Res.* **2007**, *112*, G01012. [CrossRef]
14. Tang, Q.; Peterson, S.; Cuenca, R.H.; Hagimoto, Y.; Lettenmaier, D.P. Satellite-based near-real-time estimation of irrigated crop water consumption. *J. Geophys. Res. Atmos.* **2009**, *114*. [CrossRef]
15. Mueller, B.; Seneviratne, S.I.; Jimenez, C.; Corti, T.; Hirschi, M.; Balsamo, G.; Ciais, P.; Dirmeyer, P.; Fisher, J.B.; Guo, Z.; et al. Evaluation of global observations-based evapotranspiration datasets and IPCC AR4 simulations. *Geophys. Res. Lett.* **2011**, *38*. [CrossRef]
16. Long, D.; Longuevergne, L.; Scanlon, B.R. Uncertainty in evapotranspiration from land surface modeling, remote sensing, and GRACE satellites. *Water Resour. Res.* **2014**, *50*, 1131–1151. [CrossRef]
17. Vinukollu, R.K.; Wood, E.F.; Ferguson, C.R.; Fisher, J.B. Global estimates of evapotranspiration for climate studies using multi-sensor remote sensing data: Evaluation of three process-based approaches. *Remote Sens. Environ.* **2011**, *115*, 801–823. [CrossRef]

18. Allen, R.G.; Tasumi, M.; Morse, A.; Trezza, R.; Wright, J.L.; Bastiaanssen, W.; Kramber, W.; Lorite, I.; Robison, C.W. Satellite-Based Energy Balance for Mapping Evapotranspiration With Internalized Calibration (METRIC)—Applications. *J. Irrig. Drain. Eng.* **2007**, *133*, 395–406. [CrossRef]
19. Mu, Q.; Zhao, M.; Running, S.W. Improvements to a MODIS global terrestrial evapotranspiration algorithm. *Remote Sens. Environ.* **2011**, *115*, 1781–1800. [CrossRef]
20. Tang, R.; Li, Z.-L.; Jia, Y.; Li, C.; Sun, X.; Kustas, W.P.; Anderson, M.C. An intercomparison of three remote sensing-based energy balance models using Large Aperture Scintillometer measurements over a wheat–corn production region. *Remote Sens. Environ.* **2011**, *115*, 3187–3202. [CrossRef]
21. Syed, T.H.; Webster, P.J.; Famiglietti, J.S. Assessing variability of evapotranspiration over the Ganga river basin using water balance computations. *Water Resour. Res.* **2014**, *50*, 2551–2565. [CrossRef]
22. Li, Z.; Tang, R.; Wan, Z.; Bi, Y.; Zhou, C.; Tang, B.; Yan, G.; Zhang, X. A Review of Current Methodologies for Regional Evapotranspiration Estimation from Remotely Sensed Data. *Sensors* **2009**, *9*, 3801–3853. [CrossRef] [PubMed]
23. Tang, R.; Li, Z.L.; Sun, X. Temporal upscaling of instantaneous evapotranspiration: An intercomparison of four methods using eddy covariance measurements and MODIS data. *Remote Sens. Environ.* **2013**, *138*, 102–118. [CrossRef]
24. Badgley, G.; Fisher, J.B.; Jiménez, C.; Tu, K.P.; Vinukollu, R. On Uncertainty in Global Terrestrial Evapotranspiration Estimates from Choice of Input Forcing Datasets. *J. Hydrometeorol.* **2015**, *16*, 1449–1455. [CrossRef]
25. Hu, G.; Jia, L.; Menenti, M. Comparison of MOD16 and LSA-SAF MSG evapotranspiration products over Europe for 2011. *Remote Sens. Environ.* **2015**, *156*, 510–526. [CrossRef]
26. Gokmen, M.; Vekerdy, Z.; Verhoef, A.; Verhoef, W.; Batelaan, O.; Tol, C.V.D. Integration of soil moisture in SEBS for improving evapotranspiration estimation under water stress conditions. *Remote Sens. Environ.* **2012**, *121*, 261–274. [CrossRef]
27. Ruhoff, A.L.; Paz, A.R.; Collischonn, W.; Aragao, L.E.O.C.; Rocha, H.R.; Malhi, Y.S. A MODIS-Based Energy Balance to Estimate Evapotranspiration for Clear-Sky Days in Brazilian Tropical Savannas. *Remote Sens.* **2012**, *4*, 703–725. [CrossRef]
28. Olioso, A.; Chauki, H.; Courault, D.; Wigneron, J.P. Estimation of evapotranspiration and photosynthesis by assimilation of remote sensing data into SVAT models. *Remote Sens. Environ.* **1999**, *68*, 341–356. [CrossRef]
29. Carlson, T.N.; Taconet, O.; Vidal, A.; Gillies, R.R.; Olioso, A.; Humes, K. An overview of the workshop on thermal remote sensing held at La Londe les Maures, France, September 20–24, 1993. *Agric. For. Meteorol.* **1995**, *77*, 141–151. [CrossRef]
30. Boulet, G.; Mougenot, B.; Lhomme, J.P.; Fanise, P.; Lilichabaane, Z.; Olioso, A.; Bahir, M.; Rivalland, V.; Jarlan, L.; Merlin, O. The SPARSE model for the prediction of water stress and evapotranspiration components from thermal infra-red data and its evaluation over irrigated and rainfed wheat. *Hydrol. Earth Syst. Sci.* **2015**, *12*, 7127–7178. [CrossRef]
31. Zhang, L.; Dawes, W.R.; Walker, G.R. Response of mean annual evapotranspiration to vegetation changes at catchment scale. *Water Resour. Res.* **2001**, *37*, 701–708. [CrossRef]
32. Yang, D.; Shao, W.; Yeh, J.F.; Yang, H.; Kanae, S.; Oki, T. Impact of vegetation coverage on regional water balance in the nonhumid regions of China. *Water Resour. Res.* **2009**, *45*, 450–455. [CrossRef]
33. Rodell, M.; Famiglietti, J.S.; Chen, J.; Seneviratne, S.I.; Viterbo, P.; Holl, S.; Wilson, C.R. Basin scale estimates of evapotranspiration using GRACE and other observations. *Geophys. Res. Lett.* **2004**, *31*. [CrossRef]
34. Ramillien, G.; Frappart, F.; Guntner, A.; Ngo-Duc, T.; Cazenave, A.; Laval, K. Time variations of the regional evapotranspiration rate from Gravity Recovery and Climate Experiment (GRACE) satellite gravimetry. *Water Resour. Res.* **2006**, *42*. [CrossRef]
35. Ladson, A. *Hydrology: An Australian Introduction*; Oxford University Press: Melbourne, Australia, 2008.
36. Leblanc, M.; Tweed, S.; Van Dijk, A.; Timbal, B. A review of historic and future hydrological changes in the Murray-Darling Basin. *Glob. Planet. Chang.* **2012**, *80–81*, 226–246. [CrossRef]
37. Peel, M.C.; Finlayson, B.L.; Mcmahon, T.A. Updated world map of the Köppen-Geiger climate classification. *Hydrol. Earth Syst. Sci.* **2007**, *4*, 439–473. [CrossRef]
38. Digital Elevation Model (DEM) of MDB and LEB. Available online: http://www.ga.gov.au/metadata-gateway/metadata/record/72760/ (accessed on 8 March 2017).

39. Landuse Map of MDB and LEB. Available online: http://data.daff.gov.au/anrdl/metadata_files/pb_luausg9abll20160616_11a.xml (accessed on 8 March 2017).
40. McMahon, T.A.; Murphy, R.E.; Peel, M.C.; Costelloe, J.F.; Chiew, F.H.S. Understanding the surface hydrology of the Lake Eyre Basin: Part 1—Rainfall. *J. Arid Environ.* **2008**, *72*, 1853–1868. [CrossRef]
41. McMahon, T.A.; Murphy, R.E.; Peel, M.C.; Costelloe, J.F.; Chiew, F.H.S. Understanding the surface hydrology of the Lake Eyre Basin: Part 2—Streamflow. *J. Arid Environ.* **2008**, *72*, 1869–1886. [CrossRef]
42. Van Dijk, A.I.J.M.; Renzullo, L.J.; Wada, Y.; Tregoning, P. A global water cycle reanalysis (2003–2012) reconciling satellite gravimetry and altimetry observations with a hydrological model ensemble. *Hydrol. Earth Syst. Sci.* **2014**, *18*, 2955–2973. [CrossRef]
43. Long, D.; Pan, Y.; Zhou, J.; Chen, Y.; Hou, X.; Hong, Y.; Scanlon, B.R.; Longuevergne, L. Global analysis of spatiotemporal variability in merged total water storage changes using multiple GRACE products and global hydrological models. *Remote Sens. Environ.* **2017**, *192*, 198–216. [CrossRef]
44. Zhang, Y.Q.; Chiew, F.H.S.; Zhang, L.; Leuning, R.; Cleugh, H.A. Estimating catchment evaporation and runoff using MODIS leaf area index and the Penman-Monteith equation. *Water Resour. Res.* **2008**, *44*, W10420. [CrossRef]
45. Leblanc, M.J.; Tregoning, P.; Ramillien, G.; Tweed, S.O.; Fakes, A. Basin-scale, integrated observations of the early 21st century multiyear drought in southeast Australia. *Water Resour. Res.* **2009**, *45*. [CrossRef]
46. Van Dijk, A.I.J.M.; Beck, H.E.; Crosbie, R.S.; de Jeu, R.A.M.; Liu, Y.Y.; Podger, G.M.; Timbal, B.; Viney, N.R. The Millennium Drought in southeast Australia (2001–2009): Natural and human causes and implications for water resources, ecosystems, economy, and society. *Water Resour. Res.* **2013**, *49*, 1040–1057. [CrossRef]
47. BoM. Available online: http://www.bom.gov.au/ (accessed on 15 May 2014).
48. Jeffrey, S.J.; Carter, J.O.; Moodie, K.B.; Beswick, A.R. Using spatial interpolation to construct a comprehensive archive of Australian climate data. *Environ. Model. Softw.* **2001**, *16*, 309–330. [CrossRef]
49. Australian Water Availability Project (AWAP). Available online: http://www.csiro.au/awap/ (accessed on 16 March 2014).
50. Raupach, M.R.; Briggs, P.R.; Haverd, V.; King, E.A.; Paget, M.J.; Trudinger, C.M. *Australian Water Availability Project (AWAP), CSIRO Marine and Atmospheric Research Component: Final Report for Phase 3*; Technical Report No. 013; Centre for Australian Weather and Climate Research: Canberra, Australia, 2009.
51. WaterConnect. Available online: https://www.waterconnect.sa.gov.au/ (accessed on 2 April 2014).
52. Priestley, C.H.B.; Taylor, R.J. On the Assessment of Surface Heat Flux and Evaporation Using Large-Scale Parameters. *Mon. Weather Rev.* **1972**, *100*, 81–92. [CrossRef]
53. Guerschman, J.P.; Van Dijk, A.I.J.M.; Mattersdorf, G.; Beringer, J.; Hutley, L.B.; Leuning, R.; Pipunic, R.C.; Sherman, B.S. Scaling of potential evapotranspiration with MODIS data reproduces flux observations and catchment water balance observations across Australia. *J. Hydrol.* **2009**, *369*, 107–119. [CrossRef]
54. WIRADA. Available online: http://remote-sensing.nci.org.au/u39/public/html/wirada/index.shtml (accessed on 17 March 2014).
55. Monteith, J.L. Evaporation and environment. *Symp. Soc. Exp. Biol.* **1965**, *19*, 205–234. [PubMed]
56. MOD16. Available online: http://www.ntsg.umt.edu/project/mod16 (accessed on 27 May 2014).
57. Van Dijk, A.I.J.M.; Renzullo, L.J. Water resource monitoring systems and the role of satellite observations. *Hydrol. Earth Syst. Sci.* **2011**, *15*, 39–55. [CrossRef]
58. Van Dijk, A.I.J.M. *Landscape Model (Version 0.5) Technical Description*; AWRA Technical Report 3; Water Information Research and Development Alliance/CSIRO Water for a Healthy Country Flagship: Canberra, Australia, 2010.
59. Ramillien, G.; Biancale, R.; Gratton, S.; Vasseur, X.; Bourgogne, S. GRACE-derived surface water mass anomalies by energy integral approach: Application to continental hydrology. *J. Geod.* **2011**, *85*, 313–328. [CrossRef]
60. Ramillien, G.; Seoane, L.; Frappart, F.; Biancale, R.; Gratton, S.; Vasseur, X.; Bourgogne, S. Constrained Regional Recovery of Continental Water Mass Time-variations from GRACE-based Geopotential Anomalies over South America. *Surv. Geophys.* **2012**, *33*, 887–905. [CrossRef]
61. Frappart, F.; Seoane, L.; Ramillien, G. Validation of GRACE-derived terrestrial water storage from a regional approach over South America. *Remote Sens. Environ.* **2013**, *137*, 69–83. [CrossRef]
62. Seoane, L.; Ramillien, G.; Frappart, F.; Leblanc, M. Regional GRACE-based estimates of water mass variations over Australia: Validation and interpretation. *Hydrol. Earth Syst. Sci. Discuss.* **2013**, *10*, 5355–5395. [CrossRef]

63. Ramillien, G.; Frappart, F.; Seoane, L. Application of the Regional Water Mass Variations from GRACE Satellite Gravimetry to Large-Scale Water Management in Africa. *Remote Sens.* **2014**, *6*. [CrossRef]
64. Budyko, M.I. *Climate and Life*; Academic Press: New York, NY, USA, 1974.
65. Xu, X.; Liu, W.; Scanlon, B.R.; Zhang, L.; Pan, M. Local and global factors controlling water-energy balances within the Budyko framework. *Geophys. Res. Lett.* **2013**, *40*, 2013GL058324. [CrossRef]
66. Potter, N.J.; Lu, Z. Interannual variability of catchment water balance in Australia. *J. Hydrol.* **2009**, *369*, 120–129. [CrossRef]
67. Gulden, L.E.; Rosero, E.; Yang, Z.L.; Rodell, M.; Jackson, C.S.; Niu, G.Y.; Yeh, P.J.F.; Famiglietti, J. Improving land-surface model hydrology: Is an explicit aquifer model better than a deeper soil profile? *Geophys. Res. Lett.* **2007**, *34*, L09402. [CrossRef]
68. Zhang, L.; Potter, N.; Hickel, K.; Zhang, Y.; Shao, Q. Water balance modeling over variable time scales based on the Budyko framework—Model development and testing. *J. Hydrol.* **2008**, *360*, 117–131. [CrossRef]
69. Andam-Akorful, S.A.; Ferreira, V.G.; Awange, J.L.; Forootan, E.; He, X.F. Multi-model and multi-sensor estimations of evapotranspiration over the Volta Basin, West Africa. *Int. J. Climatol.* **2015**, *35*, 3132–3145. [CrossRef]
70. Shen, H. Satellite Gravimetry in Water-Limited Environments: Applications and Spatial Enhancement. Ph.D. Thesis, James Cook University, Townsville, Australia, 28 November 2014.